ELSEVIER

Journal of Power Sources 110 (2002) 57–64

JOURNAL OF POWER SOURCES

www.elsevier.com/locate/jpowsour

Synthesis and electrochemical properties of layered Li–Ni–Mn–O compounds

Lianqi Zhang, Hideyuki Noguchi*, Masaki Yoshio

Department of Applied Chemistry, Faculty of Science and Engineering, Saga University, 1 Honjyo, Saga 840-8502, Japan

Received 26 November 2001; received in revised form 8 March 2002; accepted 26 March 2002

Abstract

An attempt to prepare solid solutions in the system of $LiNiO_2$, $LiMnO_2$ and Li_2MnO_3 was performed by heating metal acetates. The solid solutions between end members $LiNiO_2$ and Li_2MnO_3 can be successfully prepared in the overall compositional ranges. Both the structure and capacity were compared based on Rietveld analysis and electrochemical investigation on solid solutions between $LiNiO_2$ and Li_2MnO_3. The result showed that the cationic disorder as well as capacity was closely related to the ratio of Li, Mn and Ni in formula. The investigation of chronopotentiogram and ex situ XRD on the solid solutions indicated that the complex phase transitions in $LiNiO_2$ during delithiation were strongly suppressed with low Mn content (Mn/(Mn + Ni) ratio was 0.1 or 0.2) and completely suppressed with the ratio more than 0.5.

Keywords: Layered Li–Ni–Mn–O compounds; Solid solutions; Phase transitions

1. Introduction

The layered $LiNiO_2$ is an attractive cathode material for lithium ion rechargeable batteries with its relatively low cost and high capacity [1–6]. However, $LiNiO_2$ is also known for the following problems. First problem is the difficulty in the preparation of excellent electroactive $LiNiO_2$ because its electrochemical properties strongly depend on Li:Ni ratio in $LiNiO_2$, cation disorder and the oxidation state of Nickel. Secondly, $LiNiO_2$ suffers from poor cycling property when it is charged to a higher voltage (4.3 V versus Li^+/Li) for extracting more Li^+ with an appreciable volume change [3]. Several reasons responsible for it have been suggested such as microcracking or debonding of the cathode materials and the binder resulting from significant volume changes in the material accompanied by phase transitions [7,8] and decomposition of the cathode material [9–11]. In addition, the safety of cathode is also an important topic. $LiNiO_2$ is the most metastable at a charged state among three promising cathodes, $LiNiO_2$, $LiCoO_2$ and $LiMn_2O_4$, because the charged $LiNiO_2$ was reported to decompose at about 200 °C, releasing heat and oxygen [9–11].

Various attempts have been made to solve the above problems. Recently, an increasing research activity is being devoted to substituted $LiM_yNi_{1-y}O_2$ materials (M = Mn [12–21]; Mg [22–24]; Fe [25–27]; Co [28–30]; Al [31–33]; Ti [15,34,35]; B [36]; Ga [37]; and more than one transitional metal such as Mg and Ti [38]; Co, Mg and Ti [39]), since partial substitution for Nickel causes the modification of the structural and electrochemical properties of the lithium nickelates.

The solid solutions in the system of $LiNiO_2$, $LiMnO_2$ and Li_2MnO_3 might be formed because of their structural similarity. $LiMnO_2$ has orthorhombic and monoclinic structures; orthorhombic $LiMnO_2$ has corrugated layered structure which consists of an ccp oxygen array and cation sheets made up of alternating pair of Li and Mn rows; monoclinic $LiMnO_2$, which has been successfully prepared by ion-exchange technique [40], is isostructure with $LiNiO_2$ structure; Li_2MnO_3 ($Li[Li_{1/3}Mn_{2/3}]O_2$) has a layered monoclinic structure with cationic (1 1 1) plane alternatively occupied by Li and $Li_{1/3}Mn_{2/3}$ layers. Furthermore, it is believed in the system that Mn^{4+} can be introduced and act as buffer ions, which can eliminate detrimental effect of Ni^{2+}-defect in $LiNiO_2$ because tetravalent ion can help in balancing two oxygen ions and maintain both the electronic neutrality and structural integrity without the need of Ni^{2+} occupying Li sites [19,33].

Some studies on these solid solutions have been carried out. Arai et al. have reported that Manganese-substitutives indicate large capacity, good cyclability and enhanced thermal stability and were the most promising cathode [15],

* Corresponding author. Tel.: +81-952-28-8674; fax: +81-952-28-8591.
E-mail address: noguchih@cc.saga-u.ac.jp (H. Noguchi).

0378-7753/02/$ – see front matter
PII: S0378-7753(02)00169-6

although Rossen et al. first claimed detrimental effect of substituting Mn or co-substituting Li and Mn on battery performance in the system of $LiNiO_2$–$LiMnO_2$–Li_2MnO_3 [12]. Neudecker et al. [16] reported good cycling stability at a higher voltage up to 4.8 V in a thin-battery using Li and Mn co-incorporated nickelate. Recently, layered Li–Ni–Mn–O compounds with high manganese content and excellent electrochemical performances were also reported [20,21]. We have already reported that $Li_zNi_{0.9}Mn_{0.1}O_2$ and $Li_zNi_{0.8}Mn_{0.2}O_2$ can be prepared over a wide value of z using γ-MnOOH as manganese source with a constant discharge capacity of ca. 160 mAh/g [17] and manganese was determined to exist at tetravalent state in substitutives by using the high resolution X-ray fluorescence spectroscopy [18].

In this work, in order to further understand the effect of substituting Mn or co-incorporating Li and Mn in $LiNiO_2$, an attempt to prepare the solid solution in the overall compositional ranges in the system of $LiNiO_2$, $LiMnO_2$ and Li_2MnO_3 was completed under a final heating temperature of 770–870 °C in flowing oxygen. The comparison of the structural and electrochemical properties was performed on the solid solutions of $LiNiO_2$–Li_2MnO_3.

2. Experimental

Acetate compounds were used as starting materials. A stoichiometric ratio of $Ni(CH_3COO)_2{\cdot}4H_2O$ and $Mn(CH_3COO)_2{\cdot}4H_2O$ and $LiCH_3COO{\cdot}2H_2O$ were mixed and ground using a mortar and a pestle. The mixture was firstly decomposed at 400 °C in air and ground after cooling. The decomposed mixture was heated at 650 °C under oxygen atmosphere for 15 h and then ground again after cooling. The intermediate mixture was pelletized under 1000 kg/cm^2 and finally calcined at 770–870 °C in oxygen for 20 h.

The crystallography of samples and delithiated products was characterized using a Rigaku diffractometer (RINT 1000) with Cu Kα radiation. Izumi's Rietveld Program (RIETAN) [41] was used for the analysis of powder diffraction profiles.

The charge and discharge characteristics of Li–Ni–Mn–O cathodes were examined in laboratory cells. The cells were composed of a cathode and a lithium metal anode separated by a polypropylene separator and a glass fiber mat. The cathode consisted of 25 mg Li–Ni–Mn–O compound and 10 mg conducting binder pressed on a stainless steel screen at 800 kg/cm^2 and then dried at 200 °C for 4 h. The electrolyte solution was 1 M $LiPF_6$/ethylene carbonate (EC) and dimethylcarbonate (DMC). The EC and DMC were mixed in a 1:2 volume ratio. The cell was typically cycled in the voltage range of 3.0–4.3 V at a constant current density of 0.55 mA/cm^2 (40 mA/g).

3. Results and discussion

3.1. Solid solution diagram

A triangle phase diagram based on $LiNiO_2$, $LiMnO_2$ and Li_2MnO_3 compounds is presented in Fig. 1. Any composition in the diagram can be expressed as $xLi_2MnO_3{\cdot}yLiMnO_2{\cdot}(1-x-y)LiNiO_2$, which can be rewritten as a compositional formula of $Li_{(2+2x)/(2+x)}Mn_{2(x+y)/(2+x)}Ni_{(2-2(x+y))/(2+x)}O_2$ ($0 \le x+y \le 1$). Any point on the solid line parallel to the join between Li_2MnO_3 and $LiMnO_2$ in the

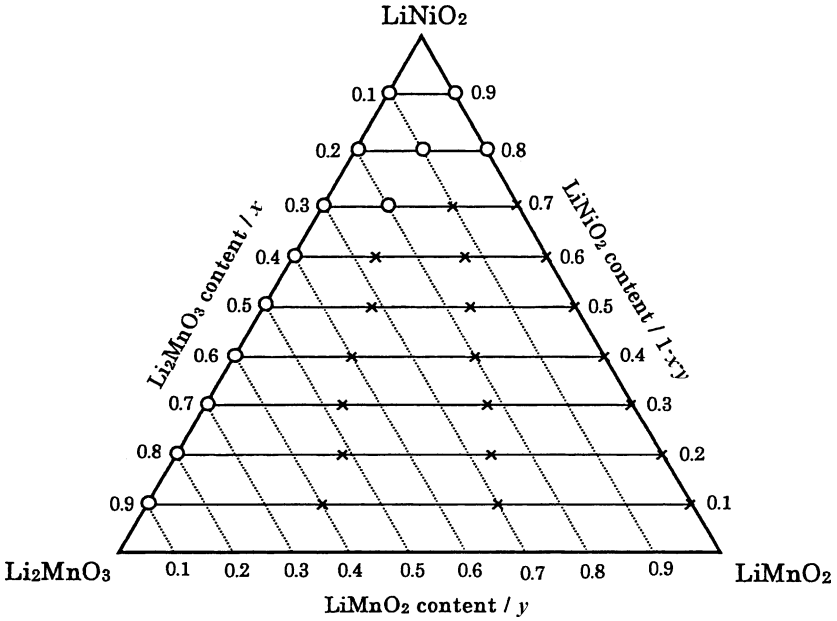

Fig. 1. Composition triangle in the system of $LiNiO_2$–$LiMnO_2$–Li_2MnO_3 (expressed as $xLi_2MnO_3{\cdot}yLiMnO_2{\cdot}(1-x-y)LiNiO_2$ or $Li_{(2+2x)/(2+x)}Mn_{2(x+y)/(2+x)}Ni_{(2-2(x+y))/(2+x)}O_2$ ($0 \le x+y \le 1$)): (○) a single phase; and (×) a mixture.

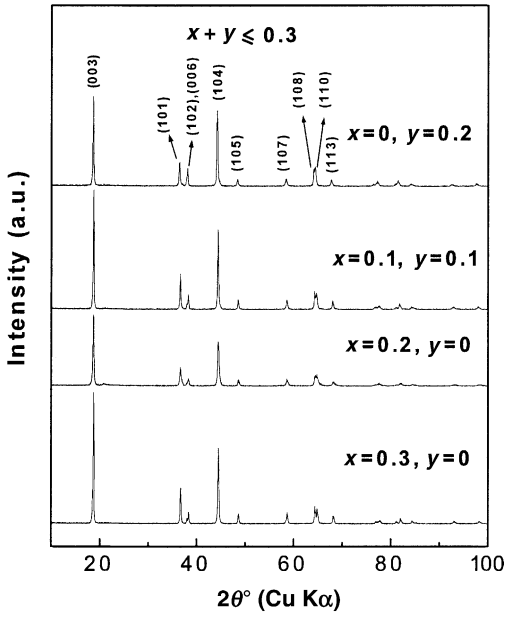

Fig. 2. The XRD patterns of several samples for $x + y \leq 0.3$.

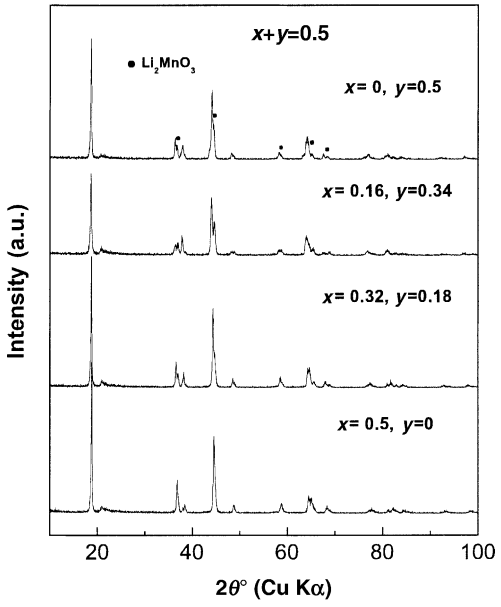

Fig. 3. The XRD patterns of samples for $x + y = 0.5$.

phase diagram has a same ratio of Mn/(Mn + Ni) ($x + y$) and any point on the dashed line parallel to the join between $LiMnO_2$ and $LiNiO_2$ has a same ratio of Li/(Mn + Ni) ($1 + x$). The points marked as the symbols (O) or (×) are the compositions that were attempted to synthesize in this work, where the circle and fork represent a single phase and a mixture, respectively. The result indicates that single-phase region lies on the range of low Mn content ($x + y \leq 0.3$) and the line between $LiNiO_2$ and Li_2MnO_3.

Fig. 2 shows X-ray diffraction patterns of several samples with low Mn content ($x + y \leq 0.3$). The patterns of samples can be identified as a single-phase with space group $R\bar{3}m$. The typical miller indices of space group $R\bar{3}m$ for all diffraction peaks are also shown in the figure. However, when Mn/(Mn + Ni) ratio $x + y$ is over 0.3, solid solutions can form only at y near zero (solid solutions between $LiNiO_2$ and Li_2MnO_3), as shown in Fig. 1.

Samples with high manganese content, $x + y = 0.5$ and 0.8, correspond to a solid line parallel to the join between Li_2MnO_3 and $LiMnO_2$ in the phase diagram, respectively. Their XRD patterns are shown in Figs. 3 and 4, respectively. A similarity between two figures can be observed. Samples with $y > 0$ contain an impure phase; the impurity decreases with decreasing y and the single-phase forms when y approaches zero. This means that the purity of sample depends on the Li/(Mn + Ni) ratio, when Mn/(Mn + Ni) ratio is fixed. The single phase can be indexed to the space group $C2/m$ (Li_2MnO_3-related). It should be noted that Li_2MnO_3 is the main impurity with $x + y \leq 0.5$ and $LiMn_2O_4$ spinel appears as an impurity and becomes a main impurity with $x + y \geq 0.6$. This is reasonable. The formation of impurities, Li_2MnO_3 and $LiMn_2O_4$, occurs at even <500 °C and the ratio of Li versus Mn at the starting compositions affects their final formation, whereas $LiNiO_2$ does not form at that temperature.

Single-phase products with $x + y \leq 0.2$ have been previously reported in detail by us [17]; here, we mainly examined the solid solutions between $LiNiO_2$ and Li_2MnO_3.

3.2. The solid solutions of $LiNiO_2$–Li_2MnO_3

3.2.1. Structure study

Refinement by Rietveld method is a good way to accurately characterize the structure and cationic distribution for $Li_{1-z}Ni_{1+z}O_2$ [4,5] and substituted lithium nickelates $Li_{1-z}(Ni_{1-y}M_y)_{1+z}O_2$ [12–15,17,20–24]. In this section, the attempt of Rietveld analysis on the solid solution domain was completed. A neutron diffraction study in rhombohedral

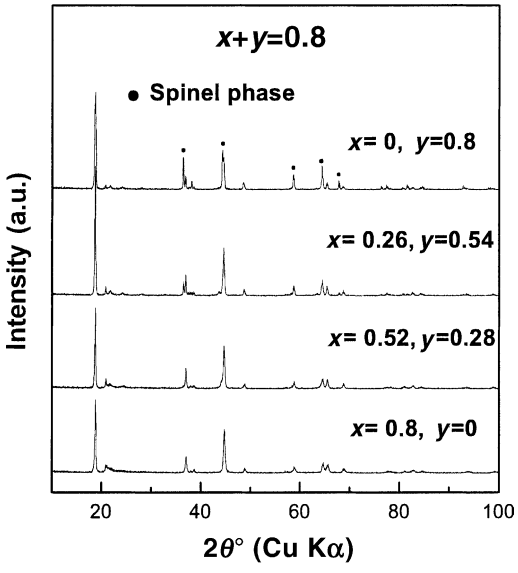

Fig. 4. The XRD patterns of samples for $x + y = 0.8$.

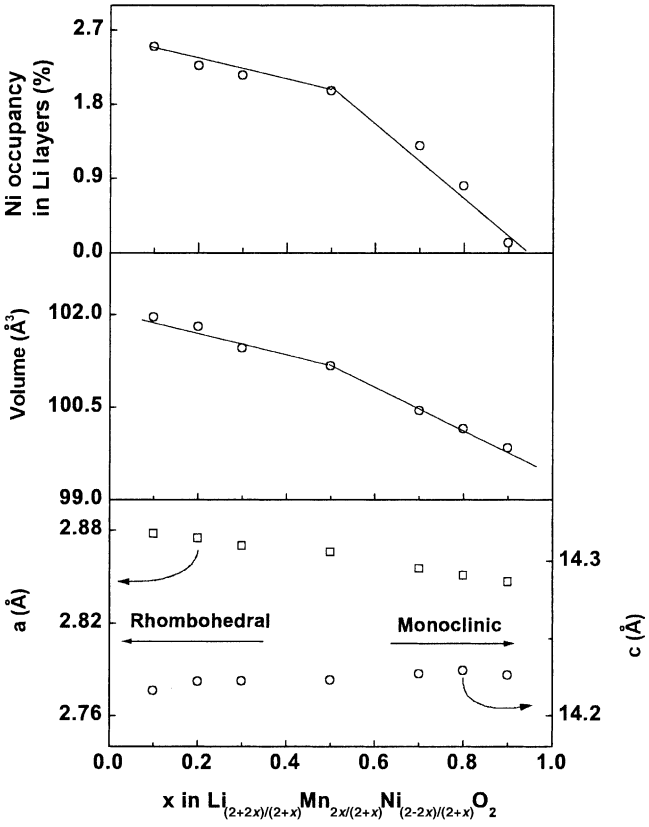

Fig. 5. The lattice constants, unit cell volume and occupancy fraction of Ni in Li layers for $Li_{(2+2x)/(2+x)}Mn_{2x/(2+x)}Ni_{(2-2x)/(2+x)}O_2$ ($0 \leq x \leq 1$).

$LiMn_{0.2}Ni_{0.8}O_2$ has showed that Mn substituted for Ni only predominately occupies Ni-filled layers of the $R\bar{3}m$ structure [14], thus the following cationic distributions are considered on Rietveld refinement: Ni and Li are allowed to present at 3a or 3b sites and Mn only at 3a sites, the total occupancy of each site is equal to unity and the ratio of Mn:Ni is equal to $x/(1-x)$.

The composition of solid solutions between $LiNiO_2$ and Li_2MnO_3 can be expressed as $Li_{(2+2x)/(2+x)}Mn_{2x/(2+x)}Ni_{(2-2x)/(2+x)}O_2$, for the case of $y = 0$. The XRD patterns of these samples show that the solid solution crystallizes in rhombohedral symmetry (space group $R\bar{3}m$) with $x \leq 0.3$ and crystallizes in monoclinic symmetry (space group $C2/m$) with $x \geq 0.5$. Based on these structures, the refinement of Rietveld analysis was carried out and all lattice parameters of monoclinic unit cell were converted to hexagonal parameters for comparison. Fig. 5 shows the lattice parameters and occupancy of Ni in Li layers for solid solutions of $LiNiO_2$–Li_2MnO_3. The hexagonal lattice parameters, a and c, change in opposition, i.e. a-axis shrinks and c-axis expands as the increase in x but the variations for a- and c-axis are within 1.2 and 0.2%, respectively. Accordingly, volume of unit cell decreases with increasing x, which is mainly attributed to the larger change of a-axis. The cationic disorder also reduces with increasing x. A sudden change of linearity for unit cell volume and cationic disorder

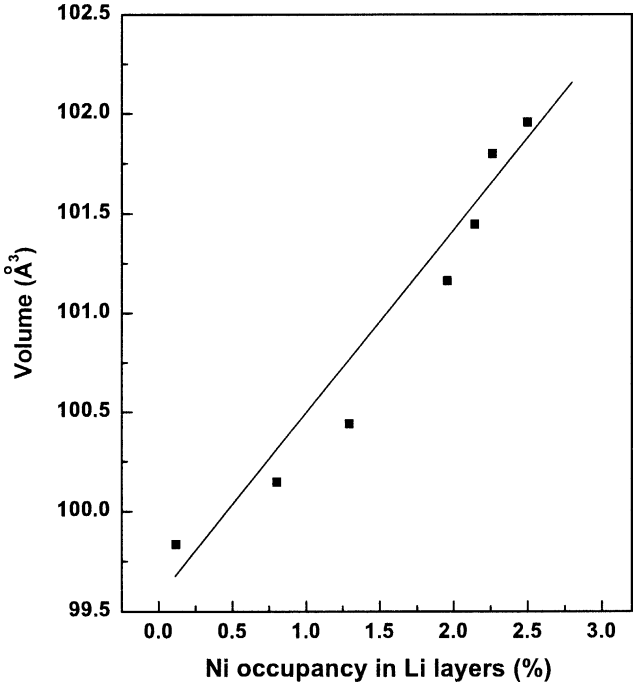

Fig. 6. Dependence of unit cell volume on Ni occupancy fraction in Li layers in the solid solution system of $LiNiO_2$–Li_2MnO_3.

is apparently observed at a same position as shown in Fig. 5, which is located at $x = 0.5$, although lattice parameters present a linear variation with compositional variation. Theoretically, unit cell volume should have a linear variation with x value, due to the linear content change of different cationic ions with a different ionic radius, in the ideal structure without cationic disorder. However, when transitional metal ions are present in Li layer, the shrinking of Li layer possibly occurs due to the smaller transitional metal ionic radius relative to lithium ion, as suggested by Delmas et al. [42]. As a result, the cationic disorder should play the other important role on the variation of unit cell volume, the change of linearity for the cationic disorder can account for change in the unit cell volume as shown in Fig. 5. When we correlate the unit cell volume with Ni occupancy in Li layers, the relation is close to linearity as shown in Fig. 6. Therefore, we believe that unit cell volume is also controlled by the Ni occupancy in Li layers in this solid solution system.

3.2.2. Electrochemical study

The initial charge–discharge curves of $Li_{(2+2x)/(2+x)}Mn_{2x/(2+x)}Ni_{(2-2x)/(2+x)}O_2$ ($0 \leq x \leq 1$) are as shown in Fig. 7. Reversible capacity decreases with increasing x, which results from the increase of average valence of transition metals and being difficult to extract more electrons from transition metals. Complex charge–discharge curves of $LiNiO_2$ are gradually replaced for simple charge–discharge curves. This becomes clear by observation of the chronopotentiograms as shown in Fig. 8. With the increase in x, the height and sharpness of peaks decrease gradually; anodic peaks at 3.797 and 4.22 V as well as small and broadened

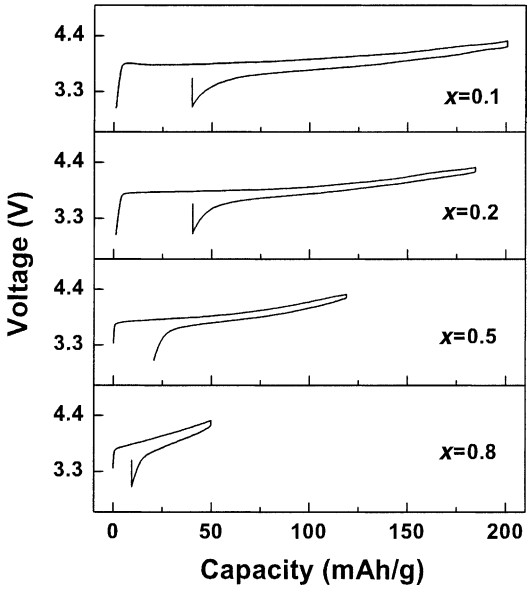

Fig. 7. Initial charge–discharge curves of partial $Li_{(2+2x)/(2+x)}Mn_{2x/(2+x)}Ni_{(2-2x)/(2+x)}O_2$ $(0 \le x \le 1)$ galvanostatically cycled between 3.0 and 4.3 V at the current density of 0.55 mA/cm^2 (40 mA/g).

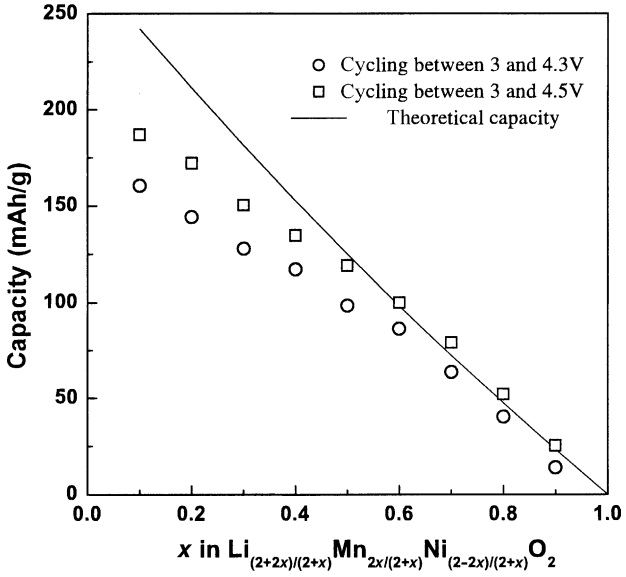

Fig. 9. Initial discharge capacity of $Li_{(2+2x)/(2+x)}Mn_{2x/(2+x)}Ni_{(2-2x)/(2+x)}O_2$ $(0 \le x \le 1)$ under different charge–discharge conditions as well as its theoretical capacity line.

cathodic peaks at 3.74 and 4.15 V can be observed for $x = 0.1$; for $x = 0.2$, only anodic peak at about 3.8 V can be clearly observed and is located at a higher peak voltage in contrast to that of $x = 0.1$; when x is 0.5, the height and sharpness of the anodic peak at about 3.8 V decrease drastically; as x increases to 0.8, no apparent peaks can be observed in its differential chronopotentiogram. This follows the phase transitions, which happen in the charge–discharge process in $LiNiO_2$ [3,4], are strongly suppressed with low x values (0.1 or 0.2) and disappear with $x \ge 0.5$.

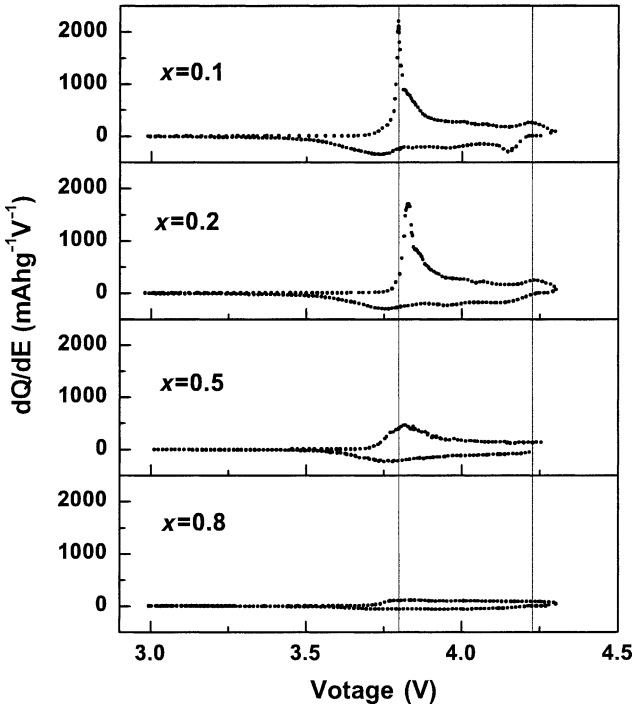

Fig. 8. Chronopotentiograms of partial $Li_{(2+2x)/(2+x)}Mn_{2x/(2+x)}Ni_{(2-2x)/(2+x)}O_2$ $(0 \le x \le 1)$.

Fig. 9 summarizes the initial discharge capacities as a function of x. In order to extract more Li^+, batteries were also charged by constant voltage and then discharged galvanostatically in the cut-off of 3.0–4.5 V at a current density of 0.55 mA/cm^2 (40 mA/g). The theoretical capacity of each sample is calculated based on the following equation assuming that Ni exists in trivalent state, Mn in tetravalent state in formula, and only Ni is involved in electrochemical reaction during the charge–discharge process as follows:

$$C_{\text{theoretical}} = \frac{26800(2-2x)}{M(2+x)} \quad (\text{mAh/g})$$

where M is the molecular weight of $Li_{(2+2x)/(2+x)}Mn_{2x/(2+x)}Ni_{(2-2x)/(2+x)}O_2$ and x is as indicated in $Li_{(2+2x)/(2+x)}Mn_{2x/(2+x)}Ni_{(2-2x)/(2+x)}O_2$. It is also shown as a line in the figure. Capacity of samples with $x \ge 0.5$ is plotted along the line of theoretical value and deviates more and more from the theoretical value in the range of $x < 0.5$.

Cyclability of partial samples with $x \le 0.3$ in the cut-off of 3.0–4.5 V is indicated in Fig. 10 and excellent cycling property is observed. Sample with $x = 0.1$ maintains 88% of initial discharge capacity and still exhibits a discharge capacity of more than 160 mAh/g after the 50th cycle; sample with $x = 0.3$ does not show any fading in discharge capacity before the 30th cycle. Whereas, other samples with $x \ge 0.4$ can cycle at a constant initial discharge capacity.

The experiment of ex situ XRD for delithiated $Li_{1.09}Mn_{0.182}Ni_{0.727}O_2$ $(x = 0.2)$ and $Li_{1.2}Mn_{0.4}Ni_{0.4}O_2$ $(x = 0.5)$ was also performed in order to further confirm if the phase transitions occur during charge process. The

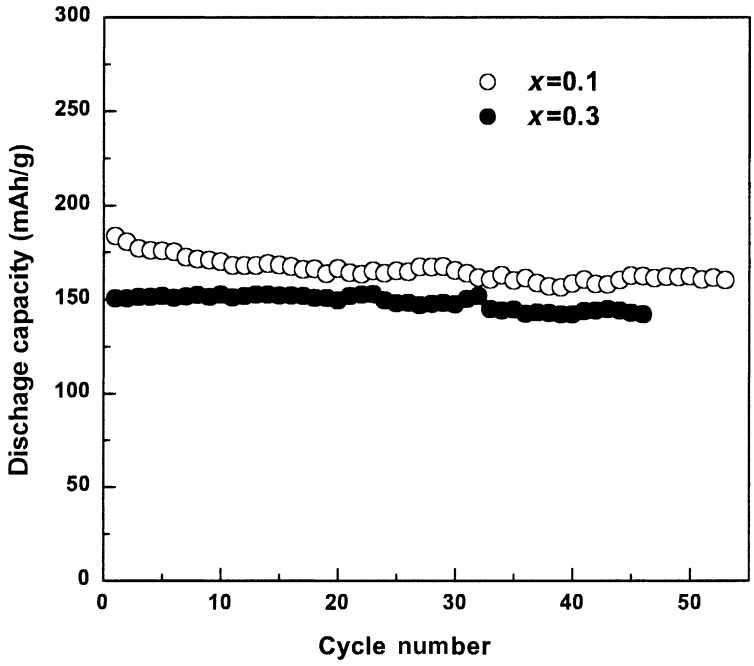

Fig. 10. Cycling performance of $Li_{(2+2x)/(2+x)}Mn_{2x/(2+x)}Ni_{(2-2x)/(2+x)}O_2$ ($x = 0.1$ or 0.3) cycled in the manner: charging to 4.5 V by constant voltage and then discharging to 3 V by constant current at a current density of 0.55 mA/cm^2 (40 mA/g).

points for ex situ XRD are selected according to the position of peaks as shown in Fig. 8. Fig. 11 shows ex situ XRD patterns for delithiated $Li_{1.09}Mn_{0.182}Ni_{0.737}O_2$. Since, the splitting in (1 0 1) and (1 0 4) peaks cannot be observed clearly and only a broadening of the (1 0 1) peak occurs, monoclinic phase does not appear during charge process [3,4]. An unusual change lies in the shift of the (0 0 3) peak and the difference between (1 0 8) and (1 1 0) peaks. The (0 0 3) peak shifts to a higher angle after shifting to a lower angle to some extent; the difference between the (1 0 8) and (1 1 0) peaks first become large and then small, which has been observed in Mg-substituted Nickelates [21]. These changes are mainly due to the c-axis: the c-axis shrinks after expansion as shown in Fig. 13. This result is consistent

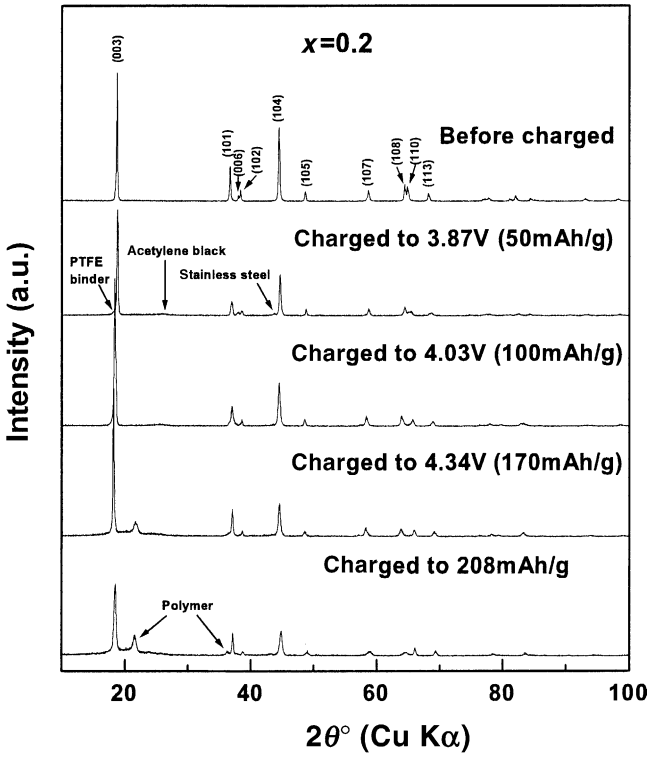

Fig. 11. The XRD patterns of delithiated $Li_{1.09}Mn_{0.182}Ni_{0.727}O_2$ ($x = 0.2$).

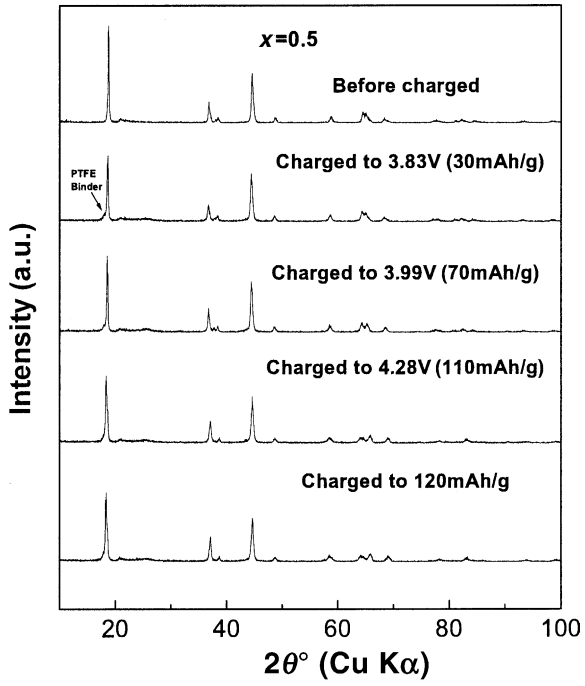

Fig. 12. the XRD patterns of delithiated $Li_{1.2}Mn_{0.4}Ni_{0.4}O_2$ ($x = 0.5$).

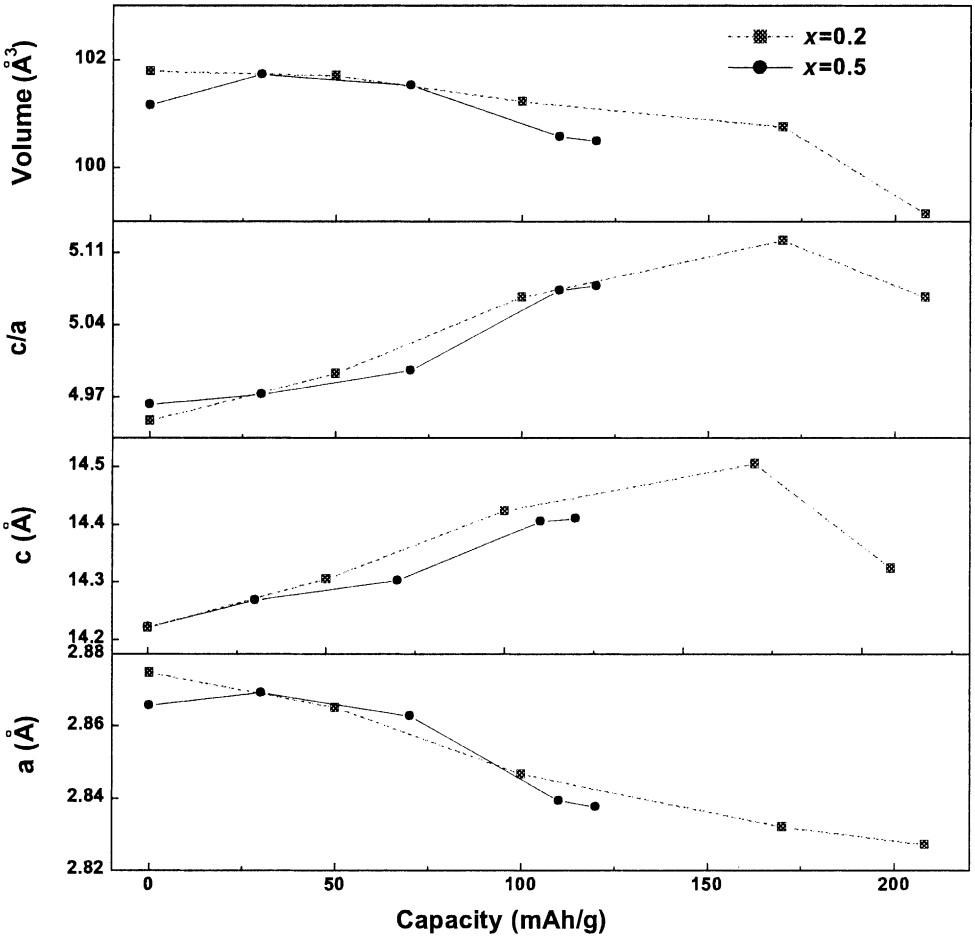

Fig. 13. Change in the lattice parameters, a and c, c/a and unit cell volume for delithiated $Li_{1.09}Mn_{0.182}Ni_{0.727}O_2$ ($x = 0.2$) and $Li_{1.2}Mn_{0.4}Ni_{0.4}O_2$ ($x = 0.5$) during the initial charge process.

with that reported previously using γ-MnOOH as Manganese source [17]. Fig. 12 shows ex situ XRD patterns for delithiated $Li_{1.2}Mn_{0.4}Ni_{0.4}O_2$. All peaks shift continuously. The unusual variation existing in $Li_{1.09}Mn_{0.182}Ni_{0.737}O_2$ does not occur in this sample. Therefore, a homogenous topotactic reaction certainly exists in the above compounds. The variation of lattice parameters, a and c, c/a, and the volume of unit cell during charge process has been summarized as shown in Fig. 13. The a-axis for every compound shrinks with delithiation due to increase in the average valence of transition metals resulting in a smaller ionic radius. The c-axis and c/a for $Li_{1.2}Mn_{0.4}Ni_{0.4}O_2$ only show expansion, whereas c-axis and c/a for $Li_{1.09}Mn_{0.182}Ni_{0.737}O_2$ show a different trend: they shrink after expansion; but only a slight shrinkage is observed in comparison with in $LiNiO_2$ [3,4]. Volume of the unit cell for every compound decreases gradually with extraction of Li^+.

4. Conclusion

The solid solutions between end members of $LiNiO_2$ and Li_2MnO_3 can be successfully prepared in the overall compositional ranges, which crystallize in rhombohedral symmetry (space group $R\bar{3}m$) with $x \leq 0.3$ and crystallize in monoclinic symmetry (space group $C2/m$) with $x \geq 0.5$. Their discharge capacity shows the good accordance to theoretical value with $x \geq 0.5$ and the gradual deviation from theoretical value with $x < 0.5$. Good cyclability for these solid solutions is also observed. Ex situ XRD investigation and chronopotentiogram indicate complex phase transitions, which happen in $LiNiO_2$, are completely suppressed with $x \geq 0.5$.

References

[1] J.R. Dahn, U. von Sacken, C.A. Michal, Solid State Ion. 44 (1990) 87.
[2] J.R. Dahn, U. von Sacken, M.W. Juzkow, H. Al-janaby, J. Electrochem. Soc. 138 (1991) 2207.
[3] T. Ohuku, A. Ueda, M. Nagayama, J. Electrochem. Soc. 140 (1993) 1862.
[4] W. Li, J.N. Reimers, J.R. Dahn, Solid State Ion. 67 (1993) 123.
[5] A. Rougier, P. Gravereau, C. Delmas, J. Electrochem. Soc. 143 (1996) 1168.
[6] T. Miyashita, H. Noguchi, K. Yamato, M. Yoshio, J. Ceram. Soc. Jpn. 102 (1994) 58.

[7] T. Ohuku, A. Ueda, Solid State Ion. 69 (1994) 201.
[8] K. Dokko, M. Nishizawa, S. Horikoshi, T. Itoh, M. Mohamedi, I. Uchida, Electrochem. Solid State Lett. 3 (3) (2000) 125.
[9] J.R. Dahn, E.W. Fuller, M. Obrovac, U. von Sacken, Solid State Ion. 69 (1994) 265.
[10] Z. Zhang, D. Fouchard, J.R. Rea, J. Power Sources 70 (1998) 16.
[11] Ph. Biensan, B. Simon, J.P. Peres, A. de Guibert, M. Broussely, J.M. Bodet, F. Perton, J. Power Sources 81/82 (1999) 906.
[12] E. Rossen, C.D.W. Jones, J.R. Dahn, Solid State Ion. 57 (1992) 311.
[13] Y. Nitta, K. Okamura, K. Haraguchi, S. Kobayashi, A. Ohta, J. Power Sources 54 (1995) 54.
[14] Y. Nitta, K. Okamura, T. Kamiyama, F. Izumi, J. Solid State Chem. 134 (1997) 1.
[15] H. Arai, S. Okada, Y. Sakurai, J. Yamaki, J. Electrochem. Soc. 144 (1997) 3177.
[16] B.J. Neudecker, R.A. Zuhr, J.D. Robertson, J.B. Bates, J. Electrochem. Soc. 145 (1998) 4160.
[17] M. Yoshio, Y. Todorov, K. Yamato, H. Noguchi, J. Itoh, M. Okada, T. Mouri, J. Power Sources 74 (1998) 46.
[18] M. Yoshio, H. Noguchi, J. Itoh, M. Okada, T. Mouri, J. Power Sources 90 (2000) 176.
[19] B.J. Neudecker, R.A. Zuhr, B.S. Kwak, J.B. Bates, J. Electrochem. Soc. 145 (1998) 4148.
[20] Z. Lu, D.D. Macneil, J.R. Dahn, Electrochem. Solid State Lett. 4 (2001) A191.
[21] T. Ohzuku, Y. Makimura, Chem. Lett. 8 (2001) 744.
[22] C. Pouillerie, L. Croguennec, Ph. Biensan, P. Willmann, C. Delmas, J. Electrochem. Soc. 147 (2000) 2061.
[23] C. Pouillerie, L. Croguennec, C. Delmas, Solid State Ion. 132 (2000) 15.
[24] C.-C. Chang, J. Yong Kim, P.N. Kumta, J. Electrochem. Soc. 147 (2000) 1722.
[25] G. Prado, A. Rougier, L. Fournes, C. Delmas, J. Electrochem. Soc. 147 (2000) 2880.
[26] J.R. Mueller-Neuhaus, R.A. Dunlap, J.R. Dahn, J. Electrochem. Soc. 147 (2000) 3598.
[27] J.N. Riemers, E. Rossen, C.D. Jones, J.R. Dahn, Solid State Ion. 61 (1993) 335.
[28] A. Ueda, T. Ohzuku, J. Electrochem. Soc. 141 (1994) 2010.
[29] I. Saadoune, C. Delmas, J. Mater. Chem. 6 (1996) 193.
[30] E. Zhecheva, R. Stoyanova, Solid State Ion. 66 (1993) 143.
[31] T. Ohzuku, A. Ueda, M. Kouguchi, J. Electrochem. Soc. 142 (1995) 4033.
[32] Q. Zhong, U. von Sacken, J. Power Sources 54 (1995) 221.
[33] G.X. Wang, S. Zhong, D.H. Bradhurst, S.X. Dou, H.K. Liu, Solid State Ion. 116 (1999) 271.
[34] S.H. Chang, S. Kang, J. Yoon, J. Choy, Solid State Ion. 86–88 (1996) 171.
[35] J. Kim, K. Amine, Electrochem. Commun. 3 (2000) 52.
[36] R. Alcantara, P. Lavela, J.L. Tirado, R. Stoyanova, E. Zhecheva, J. Solid State Chem. 134 (1997) 265.
[37] Y. Nishida, K. Nakane, T. Satoh, J. Power Sources 68 (1997) 561.
[38] Y. Gao, M.V. Yakovleva, W.B. Ebner, Electrochem. Solid State Lett. 1 (1998) 117.
[39] B.V.R. Chowdari, G.V. Subba Rao, S.Y. Chow, Solid State Ion. 140 (2001) 55.
[40] A.R. Armstrong, P.G. Bruce, Nature 381 (1996) 499.
[41] F. Izumi, Nippon Kesssho Gakkai Shi 27 (1985) 23.
[42] C. Delmas, J.P. Peres, A. Rougier, A. Demourgues, F. Weill, A. Chadwick, M. Broussely, F. Perton, Ph. Biensan, P. Willmann, J. Power Sources 68 (1997) 120.